Advanced Steel Construction – Vol. 21 No. 1 (2025) 83–94
DOI:10.18057/IJASC.2025.21.1.8

AN INNOVATIVE STEEL INTERLOCKING TIE SYSTEM FOR COMPOSITE WALLS IN MODULAR INTEGRATED CONSTRUCTION

Xiao-Kang Zou [1], Ming-Yang Li [2], Wen-Jie Lu [1,*], Jiang Huang [3], Jun Shi [3] and Yao-Peng Liu [4]

[1] *Structures Research Hub, China State Construction Engineering (Hong Kong) Ltd., Hong Kong, China*
[2] *School of Civil Engineering, Southwest Jiaotong University, Chengdu, China*
[3] *China State Construction Engineering (Hong Kong) Ltd., Hong Kong, China*
[4] *School of Civil Engineering and Transportation, South China University of Technology, Guangzhou 510641, China*
** (Corresponding author: E-mail: wenjie.lu@cohl.com)*

ABSTRACT

This paper proposes an innovative steel interlocking tie system for composite walls in reinforced concrete Modular Integrated Construction (MiC), eliminating the need for tie bolts penetrating precast sidewalls. This design facilitates complete factory interior fitting and minimizes on-site disruption to internal finishes. Experimental tests for the proposed steel interlocking system have been conducted and the advanced finite element models for the investigation of the system have been developed. Six case studies comparing density-based topology optimization and empirical optimization using finite element analysis are presented. The empirical optimization demonstrates high computational efficiency, as it does not require elaborate iterative analysis and produces a design comparable to that from topology optimization. The final optimized shape has 49.8% of the weight of the initial design and an average mechanical performance difference of 3.02% compared to the topology optimization.Six case studies comparing density-based topology optimization and empirical optimization using finite element analysis reveal that empirical optimization achieves comparable mechanical performance with significantly reduced computational cost and time. Furthermore, the system's adaptability is demonstrated through adjustments to interlocking tie dimensions accommodating to accommodate varying tying positions and wall thicknesses, effectively controlling wall deformations and meeting strength and stiffness requirements under the requirements of certain wall deformations, strength and stiffness. A successful real-world application in a Hong Kong MiC project is also presented, offering and offers practical guidance for future MiC implementations.

ARTICLE HISTORY

Received: 2 October 2024
Revised: 21 December 2024
Accepted: 22 December 2024

KEYWORDS

Modular integrated construction (MiC);
Interlocking tie system;
Finite element analysis;
Topology optimization

1. Introduction

In recent years, Hong Kong has encountered several challenges, including labor shortages, high construction costs, and significant demands for development in the construction industry. Since 2017, the Modular Integrated Construction (MiC) method has been increasingly adopted to alleviate pressure on the local construction market. This approach shifts many construction processes to prefabrication factories, significantly reducing both the duration and complexity of on-site construction.

Two primary structural systems are common in reinforced concrete MiC: column-beam frame system and shear wall system. Column-beam frame systems are prevalent in low-rise MiC modules, where adjacent modules connect with each other solely at column-beam joints using horizontal and vertical bolts. Shear wall systems, offering greater stiffness than column-beam frame systems, are typically favored in high-rise MiC modules. Although predominantly used in high-rise constructions, shear wall systems can also be beneficial in low-rise constructions due to their reduced impact on interior architectural design compared to column-beam frame systems.

This paper focuses on the shear wall structural system in reinforced concrete MiC, where shear walls are formed between adjacent modules. During on-site installation, the narrow gap between modules is filled with cast-in-situ concrete, creating a composite wall. To prevent deformation of the precast sidewalls during concrete pouring, tie rods penetrating the sidewalls are typically used to, counteracting the horizontal pressure of the wet concrete. However, this method compromises interior finishes, requiring extensive on-site repair and decoration, thus limiting its application only to projects with minimal interior design requirements, such as public housing.

Hu and Xia (2023), Ji et al. (2022), Duan et al. (2022) and Pan et al. (2023) proposed an alternative method where precast sidewalls directly resist the lateral pressure of the poured concrete without the need for tie rods. This method requires thicker precast walls to withstand the concrete pressure, consequently increasing module weight and complexity of transportation and lifting, while reducing usable interior space.

To optimize sidewall thickness and minimize disruption to factory-finished interiors, Li et al. (2023) and Yao et al. (2023) developed a composite wall system with a rebar truss tying mechanism. The rebar truss is half embedded in one precast sidewall, with the other half protruding outside the precast sidewall. By welding couplers to the protruded rebar truss to connect with tie rods, this system eliminates penetrations in one sidewall but still requires tie rods to penetrate through the other sidewall before concrete pouring. Poon et al. (2023) further refined this by embedding slotted steel angles into all the precast sidewalls, and then inserting wedge connectors into the slots from the top of the gap between two MiC modules before concrete pouring. However, the constructability and potential slippage at these slotted connections require further investigation.

To preserve interior finishes while resisting lateral pressure on thin precast sidewalls during concrete pouring, Zou et al. (2024) proposed a novel interlocking tie system for MiC composite wall construction. This new system enabling complete factory finishing and protecting interior decorations during on-site module connections, replaces the traditional through-wall tie rods. It also avoids the need for thicker sidewalls, resulting in lighter modules, increased usable space, simplified lifting, and the potential for larger module dimensions within site lifting capacity limits, ultimately enhancing occupant comfort.

To optimize the aforementioned wall tie, balancing material cost and performance requirements, the original design can be refined by adjusting material grade, geometry, and thickness. Optimization can be achieved through various methods, including manual adjustment based on numerical simulations and topology optimization. In topology optimization, the density-based method is prevalent, aiming to minimize compliance (maximize global stiffness) within a fixed domain by determining the material density of each finite element.

This optimization problem, which involves a complex integer programming formulation with variables proportional to the number of elements, can be efficiently tackled using homogenization (Bendsøe, 1989). This approach determines effective material properties for elements with microscopic voids, where the void size is related to the element density, thereby converting discrete variables into continuous ones. A crucial element of this method is the interpolation scheme that links material properties to the element density. The Solid Isotropic Material with Penalization (SIMP) method (Bendsøe, 1989; Zhou and Rozvany, 1991) is widely adopted. SIMP penalizes the element density variable to reduce element stiffness, introducing a penalty factor p (usually $p > 3$) to minimize intermediate densities, often referred to as "gray" regions, and encourage clear solid-void solutions. Although SIMP lacks a direct physical interpretation, its simplicity and effectiveness have led to its widespread use in commercial software like ANSYS.

Other topology optimization techniques go beyond the density-based method. Evolutionary Structural Optimization (ESO) (Xie and Steven, 1993, 1997) discretely adds or removes elements, and avoids intermediate densities. However, its heuristic, non-sensitivity-based criteria have been criticized for potentially leading to suboptimal solutions. Boundary variation methods, such as level set (Osher and Sethian, 1988) and phase-field (Chen, 2002) methods, define the boundary shape implicitly, often resulting in smooth boundaries that require little post-processing. Despite their advantages, these methods can

encounter difficulties when applying practical manufacturing constraints.

Note that topology optimization requiring iterative solutions of system equations demands substantial computational resources, particularly for large-scale, refined finite element models. Consequently, empirical structural optimization combined with finite element analysis, despite its potential inconsistency, is often preferred in practice for its efficiency. Therefore, this study employs both topology and empirical optimization approaches.

Based on previous systematic optimization techniques (Zou et al., 2007, 2023), this study explores both empirical and topology optimization of an innovative interlocking tie system for Modular Integrated Construction (MIC), previously successfully deployed in a real-world project. This paper also introduces the underlying mechanism of the proposed tie system. To evaluate the efficacy and reliability of empirical optimization, both empirical and density-based topology optimization are applied to interlocking tie design, and their results are compared. The broader applicability of the interlocking ties within MIC is also explored. Finally, the successful implementation of this system in a Hong Kong MiC project is presented.

2. Mechanism of the proposed interlocking tie system

The innovative interlocking tie system (Fig. 1) comprises H-shaped steel embeds, hooks, and loops, working in conjunction with MiC sidewalls to resist the lateral pressure of wet concrete during the cavity filling process between adjacent modules. The hooks and loops, featuring serrated contact surfaces (Fig. 1c), are welded to the embeds. Tie spacing is determined by factors such as lateral pressure magnitude, the loaded area per tie, and its tensile capacity.

Fig. 2 presents two MiC modules with interlocking tie system. The composite wall construction procedure is as follows:

1) Embeds are installed in the sidewalls of prefabricated modules.
2) Hooks are welded to the embeds' end plates, and loops, within loop holders, are welded to the opposing end plates.
3) The n^{th} module is installed on-site.
4) Wall reinforcement is placed between the modules. The $(n+1)^{th}$ module's loops are raised with ropes and secured to the top of the module.
5) The $(n+1)^{th}$ module is installed on-site.
6) The ropes are cut, releasing the loops to engage the hooks (Enlarged view in Fig. 2b).
7) Concrete is poured into the gap between the n^{th} and $(n+1)^{th}$ modules.

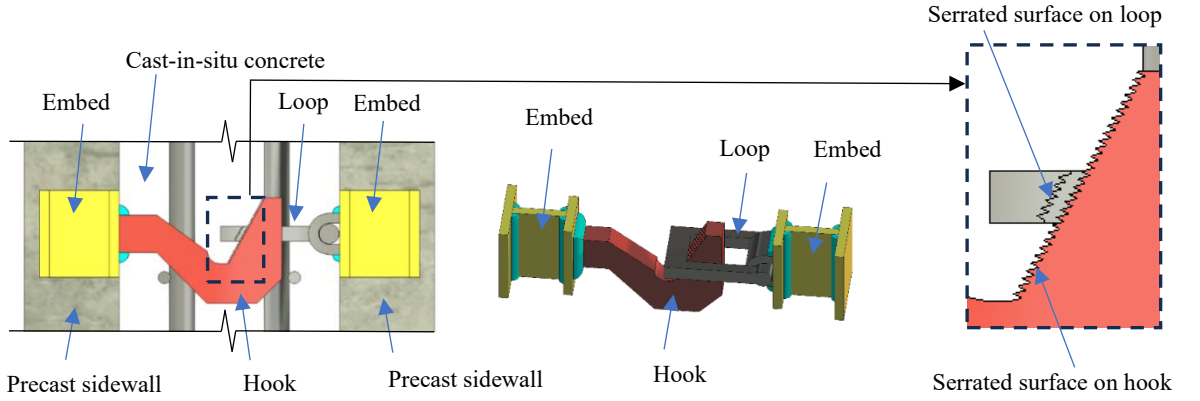

(a) Section view (b) 3D view (c) Enlarged view of interlocking details

Fig. 1 Interlocking tie system for composite walls in MiC

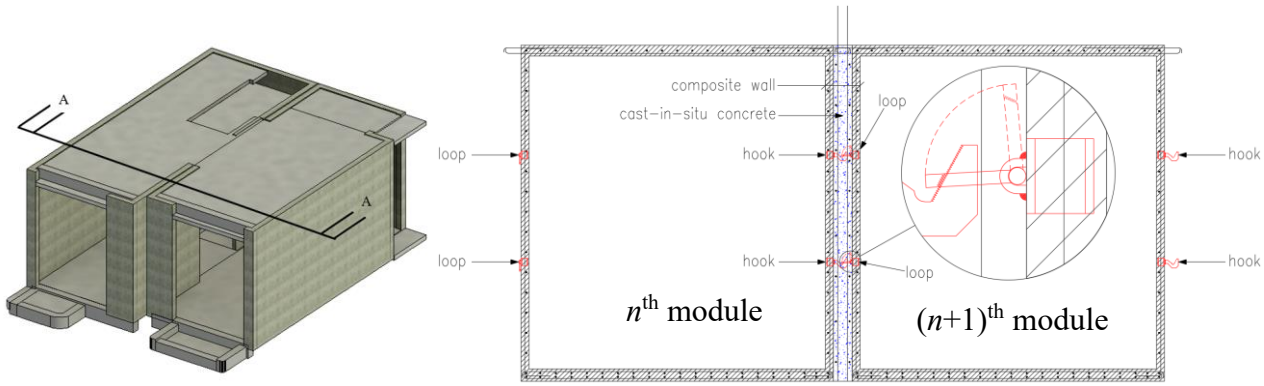

(a) BIM model (3D view) (b) Section A-A

Fig. 2 Two adjacent MiC modules with interlocking tie system

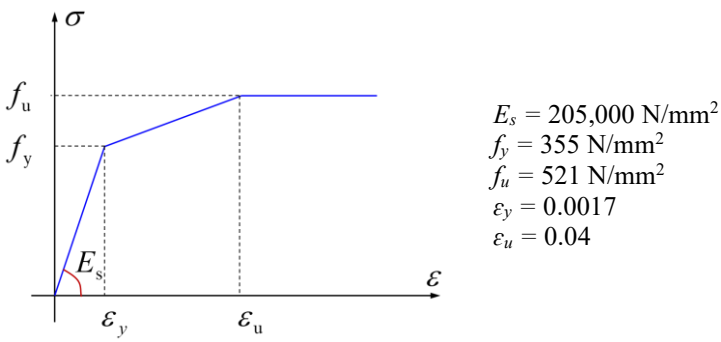

Fig. 3 Stress-strain relationship for steel material

3. Development of finite element model

In this paper, finite element analysis (FEA) models using ANSYS software were developed to investigate the behavior of the proposed interlocking tie system.

3.1. Material model of steel

The adopted S355 steel was modeled using a multilinear kinematic hardening rule (Fig. 3). The Young's modulus E_s, yield strain ε_y, ultimate strain ε_u and their corresponding yield strength f_y and ultimate strength f_u are determined from experimental tests, as illustrated in Fig. 3.

3.2. Design loads for interlocking tie system

According to the design concrete pressure envelope (Fig. 4) and the following Eq. (1) in CIRIA Report 108 (Clear and Harrison, 1985), the concrete fluid pressure acting on the sidewall of the module experiences a linear increase to P_{max} at a depth of P_{max}/D, and keeps this value to the bottom level.

$$P_{max} = \min\{D\left[C_1\sqrt{R} + C_2K\sqrt{H - C_1\sqrt{R}}\right], Dh\}, \text{ in kN/m}^2 \quad (1)$$

in which, C_1 is the coefficient dependent on the size and shape of formwork; C_2 is the coefficient dependent on the constituent materials of the concrete; D is the weight density of concrete; H is the vertical form height; h is the vertical pour height; R is the rate at which the concrete rises vertically up the form; K is the temperature coefficient taken as $(\frac{36}{T+16})^2$; T is the concrete temperature at placing.

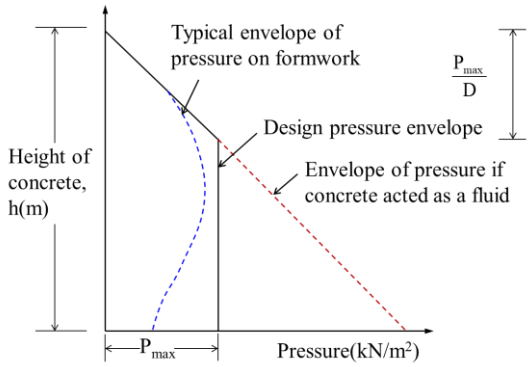

Fig. 4 Concreting pressure recommended in CIRIA report 108

In this paper, the lateral concreting pressure P_{max} can be determined by Eq. (1) and the associated parameters are given in Table 1. The distribution of concreting pressure for designing the proposed interlocking tie system is shown in Fig. 5.

Table 1
Parameters for determination of concreting pressure in this paper

Parameter	C_1	C_2	D kN/m³	H m	H m	T °C	K	R m/hr	P_{max} kPa	P_{max}/D m
Value	1.0	0.3	24.0	2.925	2.925	30	0.612	1.0	30.11	1.25

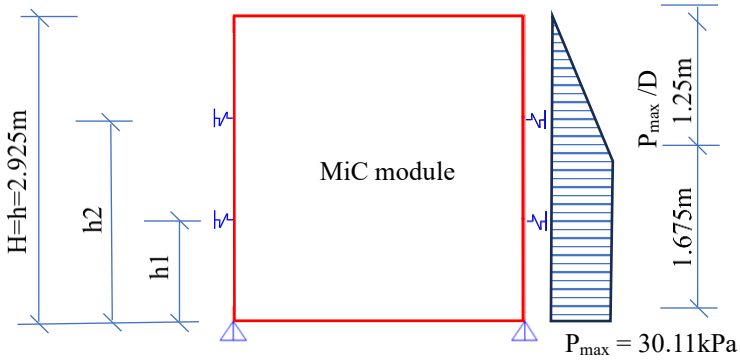

Fig. 5 Concreting pressure for designing interlocking tie system

Assuming a maximum spacing of 1.0 m vertically and horizontally for the interlocking ties, the tensile force F acting on each tie can be estimated using Eq. (2) below.

$$F = P_{max} \times \text{Loaded Area} \quad (2)$$

Taking the loaded area as 1.0m×1.0m, the tensile force F is calculated to be 30.11 kN. To estimate preliminary interlocking tie dimensions, a simplified method is used to assess key sections under combined axial, bending, and shear forces in accordance with local design codes. A worst-case unfactored tensile force F is applied to the top of the hook (Fig. 6a), and sections I-I through IV-IV (Fig. 6a, Table 2) are adjusted to meet code requirements. For the loop, F is applied to the left end (Fig. 6b). These preliminary dimensions (Fig. 6a and 6b) serve as the starting point for member size optimization.

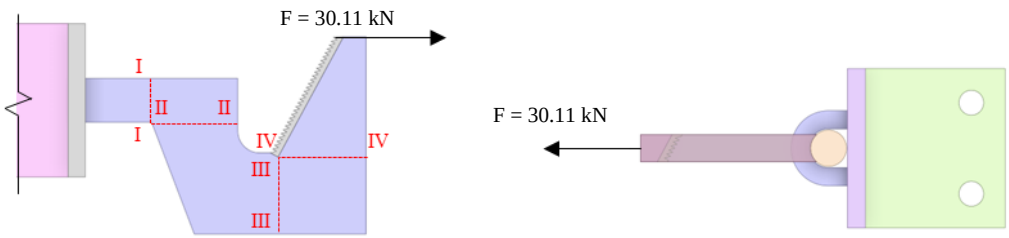

(a) Sketch of hoop component (b) Sketch of loop component

Fig. 6 Sketch of the main components of interlocking tie

Table 2
Dimensions of interlocking tie before optimization

Cross-section	Section width (mm)	Section thickness (mm)
I-I	20	30
II-II	40	30
III-III	40	30
IV-IV	40	30
Weight = 1.65 kg		

Note: The locations of cross-section I-I to IV-IV are shown in Fig. 6a.

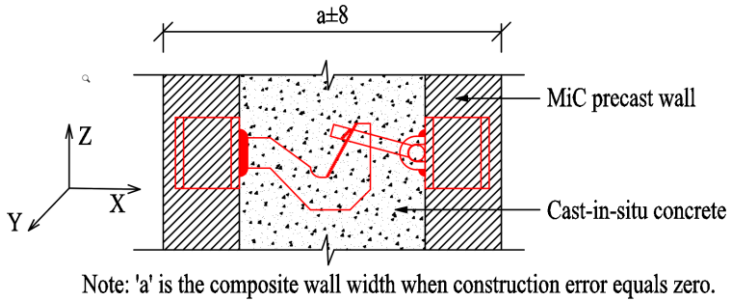

Fig. 7 Allowable construction tolerance in X direction for the interlocking tie system

3.3. Construction tolerances

Construction tolerances must be considered for embed installation, hook/loop welding (factory), and module placement (on-site). Based on practical experience, ±3 mm and ±5 mm tolerances are allocated for factory fabrication and on-site installation, respectively. Therefore, a total tolerance of ±8 mm is incorporated into the tie system design in the X-direction (Fig. 7), with similar consideration in the perpendicular horizontal Y-direction.

3.4. Finite element modeling

The concrete, steel, and rebar were modeled using a 10-node tetrahedral element in ANSYS, with three translational degrees of freedom (UX, UY and UZ) per node. The element supports plasticity, creep, swelling, stress stiffening, large deflections, and large strains. Specifically, it was used to model the steel plate in the wall tie analysis.

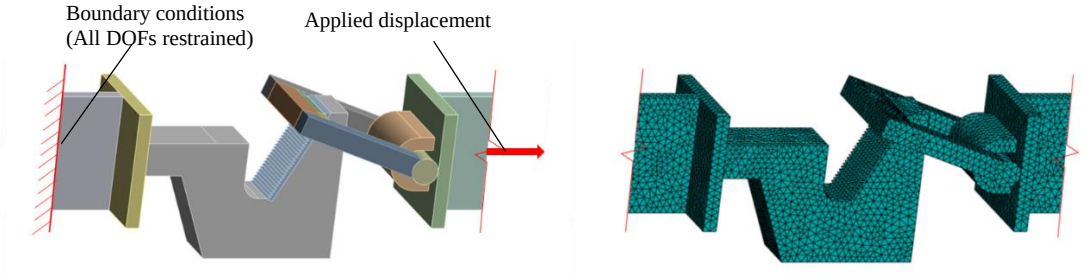

(a) Boundary conditions and applied displacement (b) Meshing details

Fig. 8 Finite element model of the interlocking tie

The interlocking tie, consisting of a hook, loop, and embedded end plates (see Fig. 6 and Table 2), connects via interlocking serrated surfaces. To simulate tensile loading, one end is fixed, while the other is displaced longitudinally until failure. Displacement restraints are applied to the left end, and a tensile displacement is applied incrementally to the right-end plate (Fig. 8a). Mesh details are shown in Fig. 8b.

The reaction force at the fixed (left) end is recorded during right-end displacement. The interlocking mechanism is modeled by coupling nodes at the serrated contact surfaces, assuming full contact and no relative movement. The loop shaft is modeled as a frictionless revolute joint.

To protect interior finishes, a maximum allowable horizontal deformation of 4 mm per sidewall during concrete pouring is considered reasonable, resulting in a total allowable deformation of 8 mm (4 mm × 2) for analysis and design.

3.5. Validation of finite element model

Experimental tensile tests were conducted to validate the finite element model developed in Section 3.4. Fig. 9 compares the force-displacement curves from both the numerical model and experiments. While the numerical model overestimates the initial stiffness (up to 8 mm displacement), likely due to the slippage of the sawtooth contact part of the specimen during the initial test loading, it accurately predicts the wall tie behavior after 8 mm, corresponding to full serration engagement. Therefore, the numerical model is deemed suitable for studying the wall tie's mechanical properties.

The validated numerical model can therefore be used for subsequent structural optimization. The physical test showed interlocking tie failure at 21 mm displacement, with rupture occurring at the loop corner (Fig. 10a). The equivalent plastic strain distribution (Fig. 10b) confirms strain concentration at the observed rupture location. Since the hook remained largely elastic during failure, indicating inefficient material usage, optimizing its shape could improve material utilization.

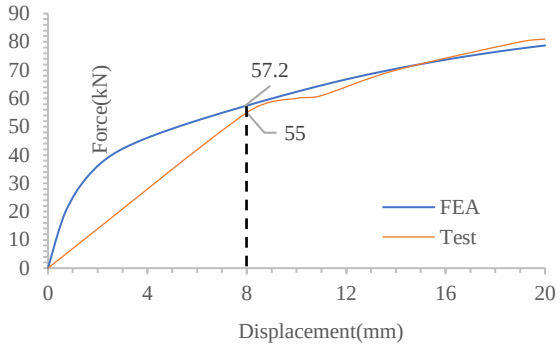

Fig. 9 Force-displacement curves from FE model and tensile test

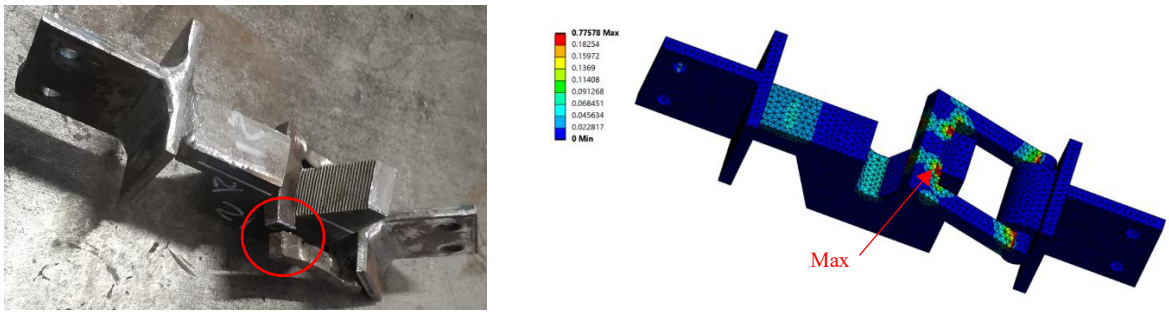

(a) Failure mode in experimental test (b) Equivalent plastic strain in FE model

Fig. 10 Failure of interlocking tie: experimental vs. numerical

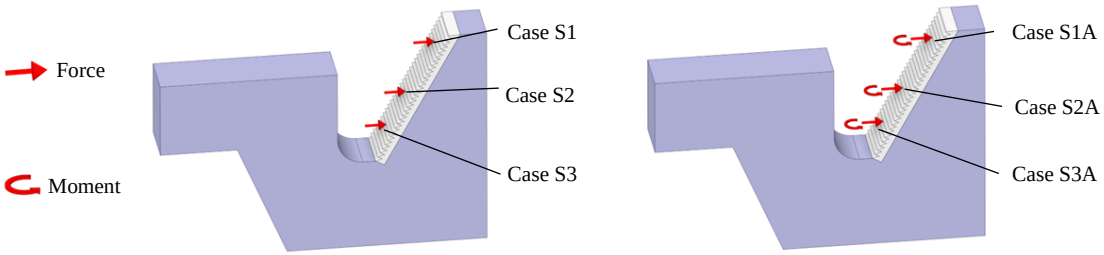

(a) Load cases without eccentricity (b) Load cases with eccentricity

Fig. 11 Critical load cases considered in optimization

4. Optimization of interlocking tie

4.1. Critical load cases for optimization

The optimization objective is to minimize the interlocking tie size while maintaining deformation within the allowable limit u_{max} under a factored applied tensile load F^d of 34.6 kN = 1.15 × F in Eq. (2). As shown in Fig. 11, based on different locking positions and eccentricities, six critical load cases are considered and listed in Table 3.

Table 3
Definition of six critical cases considered

Locking Position	Without Eccentricity	With Eccentricity
Upper	Case S1	Case S1A
Center	Case S2	Case S2A
Lower	Case S3	Case S3A

4.2. Methodology for optimization

The optimization aims to minimize wall tie volume while maintaining sufficient strength. Starting with an initial volume (V_{ini}), the design volume is iteratively reduced. The optimization converges when the minimum reaction force across all six load cases (at u_{max} displacement) equals the target applied load F^d.

Note that the initial hook design (Section 3.2) was modified by reducing the thickness from 30 mm to 20 mm and increasing the root height to 30 mm. This adjustment aimed to reduce overall stiffness and strength while preserving strength at the critical weak point.

Density-based topology optimization is employed in each iteration to determine the optimal shape for a given volume, minimizing structural compliance (and thus displacement) within the design domain under the prescribed loading.

The classical compliance minimization problem for single load case is given below:

$$\min_{\rho}[c(\rho)] = U^{T}K(\rho)U \tag{3}$$

$$\text{Subject to: } K(\rho)U = F \tag{4}$$

$$\sum_{e=1}^{N} v_e\rho_e \le V \tag{5}$$

$$\rho_{min} \le \rho_e \le 1, e = 1 \cdots N \tag{6}$$

where ρ is the vector of element design densities; ρ_e represents the density of each element; U is the displacement vector; F is the force load vector; c is the objective function which represent compliance here; $K(\rho)$ is the global stiffness matrix which varies according to ρ; v_e is the volume of each element and N is the total number of elements; V represents the volume limitation, where $V = v_f V_0$, V_0 is the volume of design domain and v_f is the fraction of the remaining volume.

Eq. (3) presents the objective function, which minimizes compliance (strain energy) to maximize overall stiffness. Eq. (4) enforces force equilibrium. Eq. (5) constrains the total element volume (V). Eq. (6) defines the upper and lower bounds for element densities.

The relationship of stiffness K and element density ρ is given by Solid Isotropic Material with Penalization (SIMP) method, introduced by Bendsøe (1989):

$$\mathrm{K}(\rho) = \sum_{e=1}^{N} \mathrm{K}_e(E_e) \tag{7}$$

$$E_e = \rho_e{}^p E^0 \tag{8}$$

in which E_e is the isotropic material property (Young's modulus in this case); p is the power-law factor used to penalize intermediate densities between 0 and 1, typically set to 3.

Eq. (7) represents the assembly of the global stiffness matrix. Eq. (8) defines the penalized proportional material properties of the elements.

For multiple load cases, the objective function is defined as the sum of the compliances for each case, as shown in Eq. (9), using the individual compliance calculations from Eq. (3):

$$\min_{\rho}[C(\rho)] = \sum_{i=1}^{N_c} c_i(\rho) \tag{9}$$

where $c_i(\rho)$ is the compliance of case i calculated using Eq. (3); and N_c is the number of load cases considered. In this paper, N_c is taken as 6, as shown in Table 3.

4.3. Empirical optimization method

The empirical optimization presented here is based on FEA results, iteratively removing material from regions exhibiting low stress and strain, as illustrated in Fig. 12.

The empirical optimization procedure is as follows:

1) Perform FEA on the initial design (Section 4.2) to identify the optimization region and determine F_{min} (the minimum reaction force across all load cases).
2) Divide the design boundary into movable and immovable segments.
3) Adjust the movable segments (via translation or rotation) while maintaining overall shape integrity, and update the FE models.
4) Perform FEA on the updated model and calculate F_{min}. Compare F_{min} with the target reaction force F_{tar} (equal to the applied load F^d from Section 4.1).
5) Repeat steps 3 and 4 until the difference between F_{min} and F_{tar} is less than 5%.
6) Compare the current volume (V_i) with the previous volume (V_{i-1}). If the difference is less than 5%, the optimization converges; otherwise, adjust the boundary based on FEA results and reaction forces, and return to step 3.

The flow chart is shown in Fig. 13.

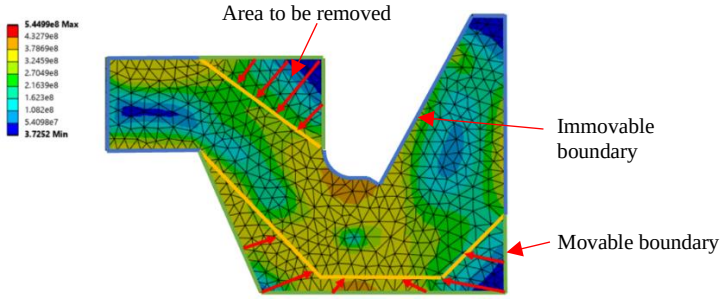

Fig. 12 Region under low stress to be removed

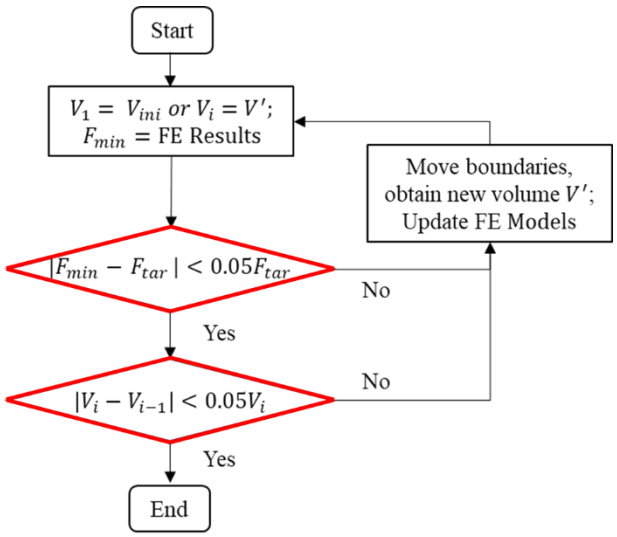

Fig. 13 Flow chart for empirical optimization

4.4. Topology optimization method

A topology optimization, employing the density-based method (Eqs. 3 to 9) within ANSYS's structural optimization module, was conducted to validate the accuracy and efficiency of the empirical optimization results. A convergence accuracy of 0.1% was used for each iteration. To ensure manufacturability with a single-directional cut and prevent the formation of voids, an extrusion constraint along the y-axis with a minimum member size of 20 mm was applied (Fig. 14).

The topology optimization process iteratively performs FEA on shapes generated with varying mass retention percentages. The objective is to identify the minimum volume shape that satisfies the design requirements. Since topology optimization results in a discrete distribution of element densities, producing a non-smooth boundary, post-processing (smoothing and linearization) is necessary to create a manufacturable component.

The topology optimization procedure is as follows:

1) Starting with the initial design (Section 4.2), define the optimization and excluded regions. Apply load cases and manufacturing constraints (minimum member size and extrusion direction).
2) For the first cycle, set the initial volume retention ratio (V_{ini}) to 90% and the volume reduction step size ($V_{st,ini}$) to 5%. Subsequent cycles update V_f (volume retention ratio) and V_{st} (step size).
3) Employ the topology optimization algorithm (Eqs. 3 to 9) to calculate compliance and update element densities. Interpret the resulting material distribution as the updated design.
4) Perform FEA on the updated model and compare F_{min} with F_{tar}. If $F_{min} < F_{tar}$, reduce V_f by V_{st}. If $F_{min} > F_{tar}$, reduce the step size to $V_{st}' = 0.5V_{st}$.
5) Repeat steps 3 and 4 until the difference between F_{min} and F_{tar} is less than 5%.
6) Compare the current volume fraction ($V_{f,i}$) with the previous ($V_{f,i-1}$). If the difference is less than 5%, the optimization converges; otherwise, reduce the step size to $V_{st}' = 0.5V_{st}$ and return to step 2.

The topology optimization procedure is illustrated in Fig. 15.

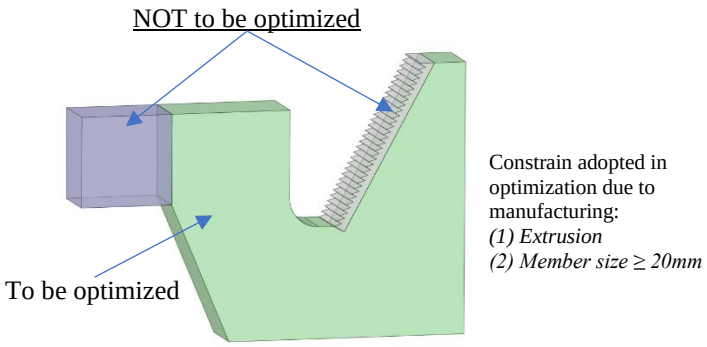

Fig. 14 Settings for topology optimization

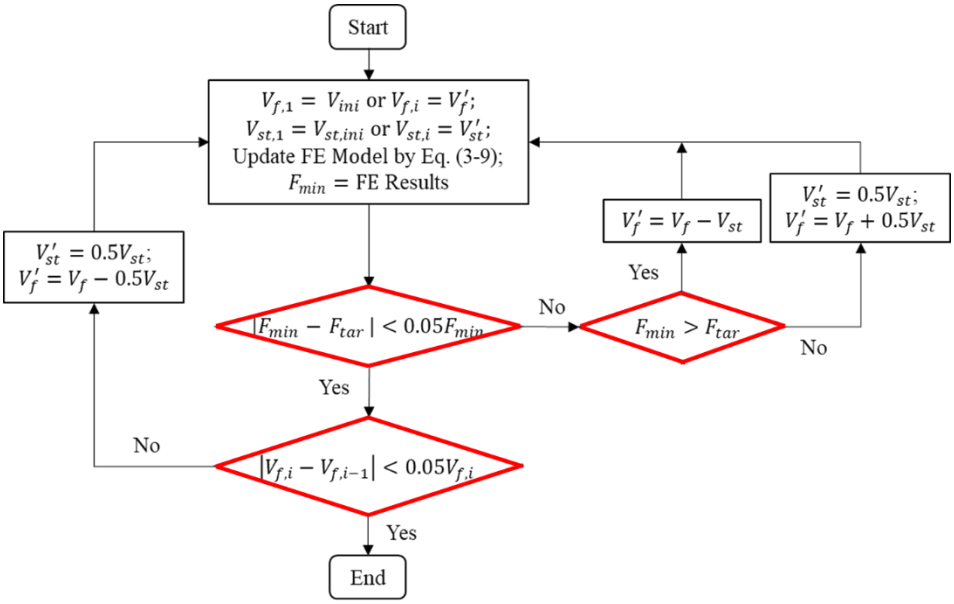

Fig. 15 Flow chart for topology optimization

4.5. Result comparison between two optimization methods

4.5.1. Optimization history

The steel weight and reaction force for achieving design loads during optimization in two different methods are shown in Fig. 16.

The empirical optimization converged in 6 cycles, while the topology optimization required 9 cycles. The final design, based on a linearization of the Cycle 8 and Cycle 9 results, weighs 814 g, a value between the weights of those two cycles.

The stress distribution during optimization processing is demonstrated in Table 4.

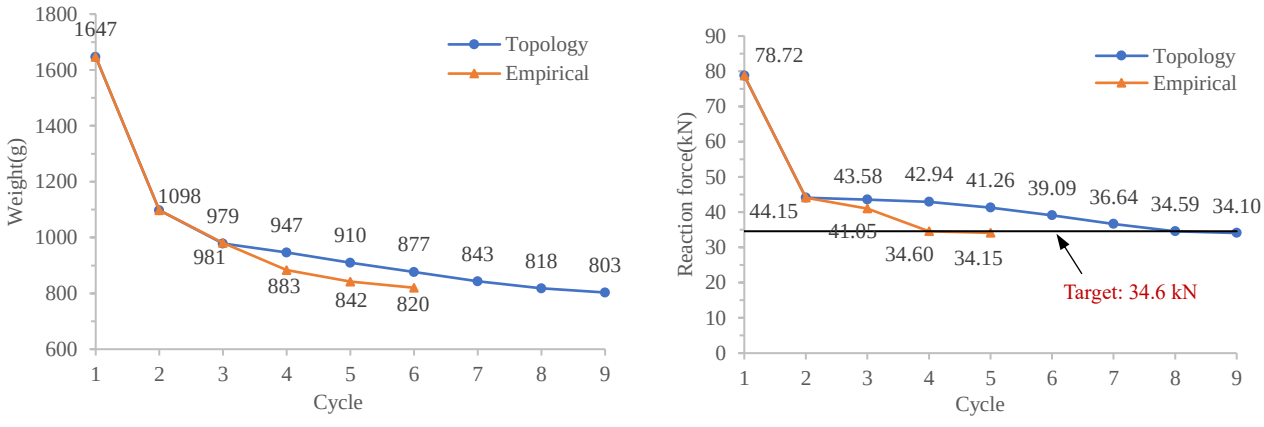

(a) Steel weight

(b) Reaction force

Fig. 16 History of two optimization methods

Table 4
Stress distribution for representative cycles in topology optimization method

Equivalent stress	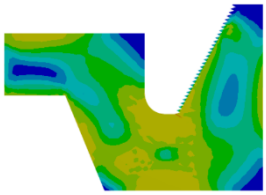	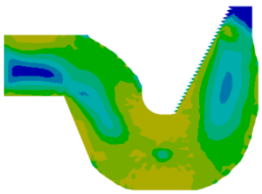	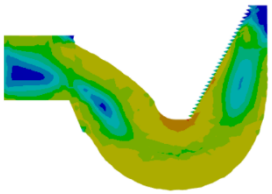	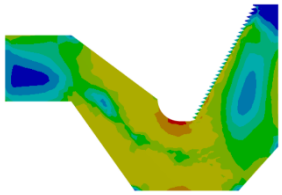
Cycle No.	2	3	9	Final

4.5.2. Comparison of steel weight

The designs from both empirical and topology optimization are shown in Fig. 17. The empirical optimization design weighs 820 g, which is 49.8% of the initial weight. In contrast, the topology optimization design weighs 814 g, representing 49.4% of the initial weight.

4.5.3. Comparison of section dimensions

Fig. 17 illustrates the differences between the results of the two optimization methods. Although the overall shape remains consistent, the dimensions of the cross-sections have changed, particularly in sections II'-II' and III'-III'. The maximum difference in cross-sectional area is 9.1%.

4.5.4. Comparison of stress distribution

The stress distribution of original design is compared against that of the topology optimization and empirical optimization in Fig. 18.

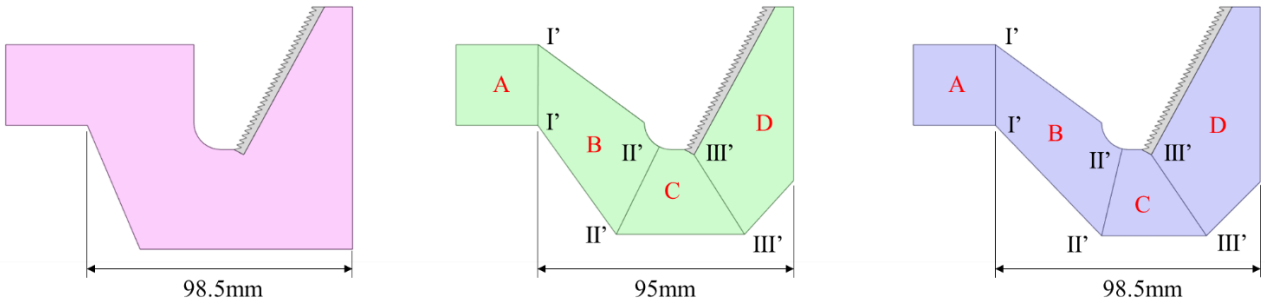

(a) Original design (b) Topology optimization (c) Empirical optimization

Fig. 17 Dimensions of interlocking tie before and after optimization

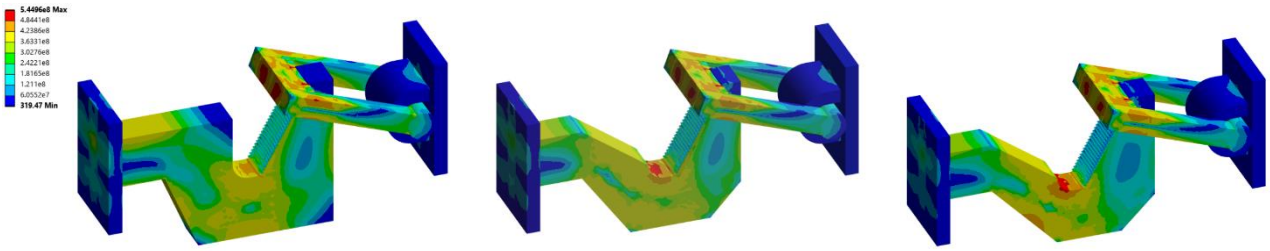

(a) Original design (b) Topology optimization (c) Empirical optimization

Fig. 18 Stress comparison before and after optimization

4.5.5. Comparison of load-deflection curves

Finite element analysis (FEA) was conducted on both optimization schemes using the validated model. As shown in Fig. 19, the two schemes yield almost identical weights and similar mechanical properties, with an average tensile force difference of 3.02% at 8 mm displacement and a maximum difference of 6.5% in Case S1A. The primary distinction between the schemes is the location of yielding, attributed to variations in cross-section dimensions.

This demonstrates that empirical optimization is acceptable for practical engineering, as it saves computational effort and converges faster while maintaining accuracy comparable to topology optimization algorithms.

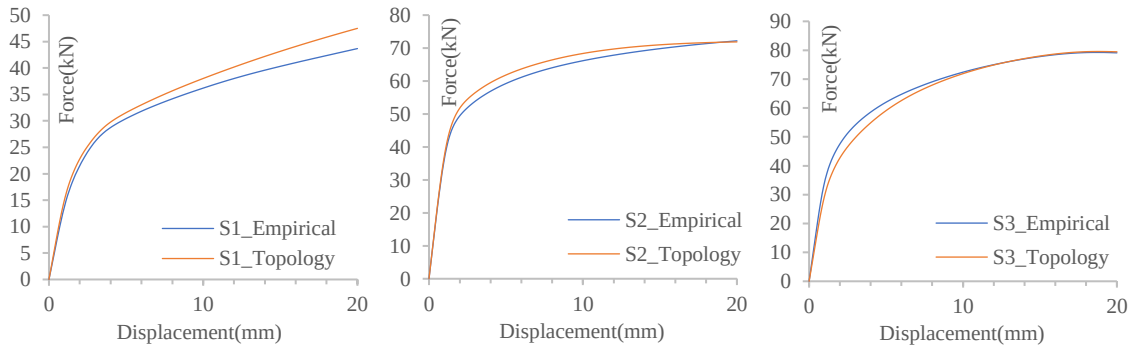

(a) Case S1 (b) Case S2 (c) Case S3

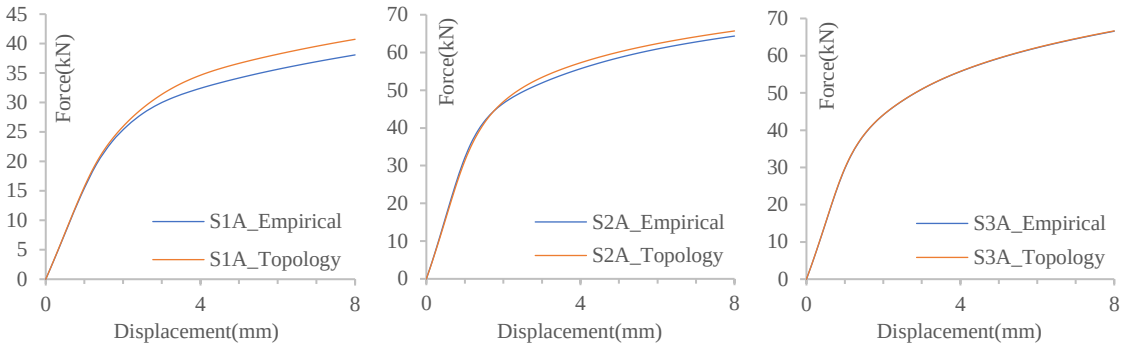

(a) Case S1A (b) Case S2A (c) Case S3A

Fig. 19 Load-deflection curves from empirical and topology optimization methods

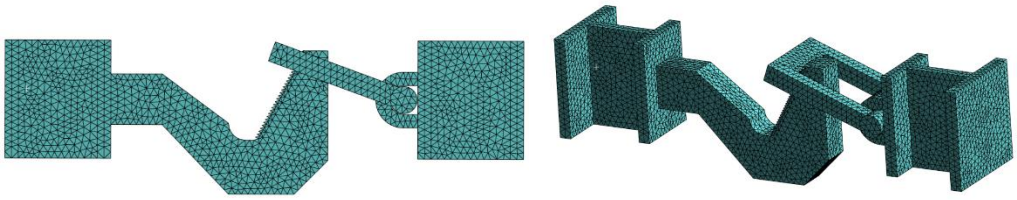

(a) Section view (b) 3D view

Fig. 20 Final optimized shape of the interlocking tie

4.5.6. Final optimized shape of interlocking tie

The optimized shape and finite element model are shown in Fig. 20. The model uses the shape obtained through the empirical optimization procedure outlined in Section 4.3 and follows the model settings described in Section 3.6.

4.5.7. Verification test against numerical analysis – Case S1

Additional experimental tensile test for Case S1 after empirical optimization was conducted. The force-displacement curves in Fig. 21 indicate that the numerical results closely match the tensile test after 5 mm of displacement. Initially, during the first 5 mm, the numerical model shows higher stiffness than the experimental test, as the idealized contact assumed in the FE model does not fully account for the slippage of the sawtooth contact part of the specimen during the initial loading. Fig. 22 compares the deformed shapes of the test sample with the numerical model.

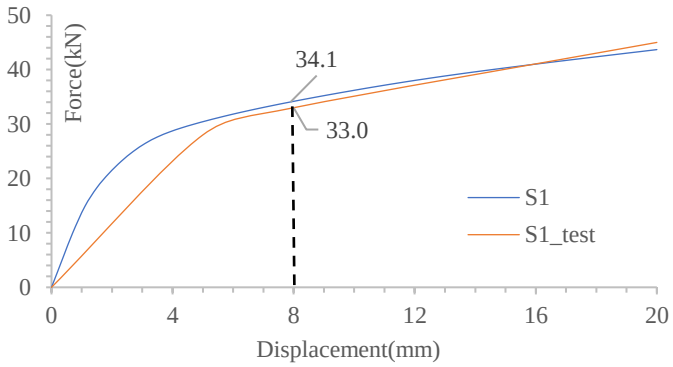

Fig. 21 Force-displacement curves for Case S1 (empirical optimization)

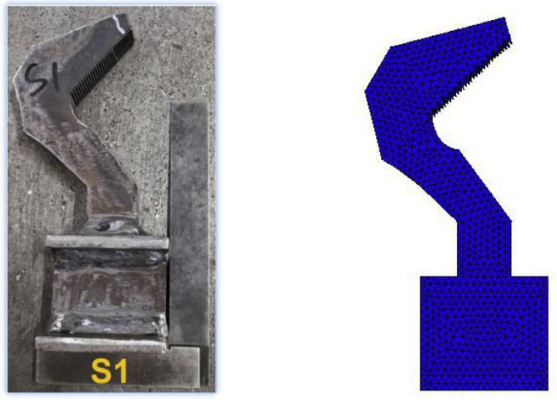

(a) Deformed shape after testing (b) Deformed shape from FEA

Fig. 22 Comparison of deformed shapes for Case S1 (empirical optimization)

5. Influence of tie location and wall thickness

5.1. Effect of interlocking tie location along the height of composite wall

According to the analysis in Section 3, changes in height due to position variation primarily influence the force change in the wall tie. This section focuses on the design of the interlocking tie when the height h_2 is 2.0 m. When the height changes to h_2 = 2.0 m, the tension force reduces to about 85% of that at h_1=1.0m.

To meet lower stiffness and load-carrying capacity requirements, the hook size can be reduced while maintaining its basic shape. When the required tensile force at an 8 mm displacement along X-axis is reduced to about 85% of the final scheme, the size-reduced hook is shown in Fig. 23. This hook weighs 568.8 g, which is 76.6% of the weight in the empirical optimization scheme.

The force-displacement curves for six critical load cases from numerical analysis are shown in Fig. 24. It can be seen that the overall trend of the curve is similar to the scheme before the position change. However, the tension is reduced by approximately 14% when the displacement reaches 8 mm.

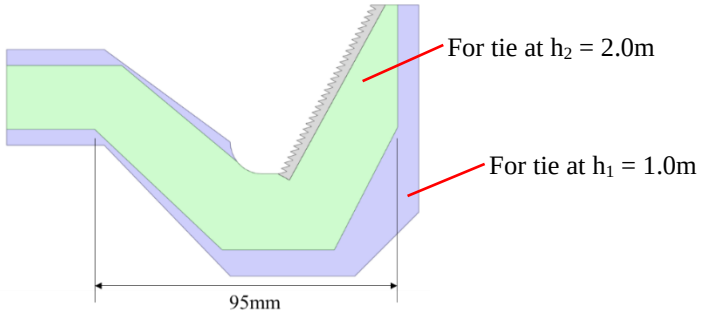

Fig. 23 Design of interlocking tie at different locations

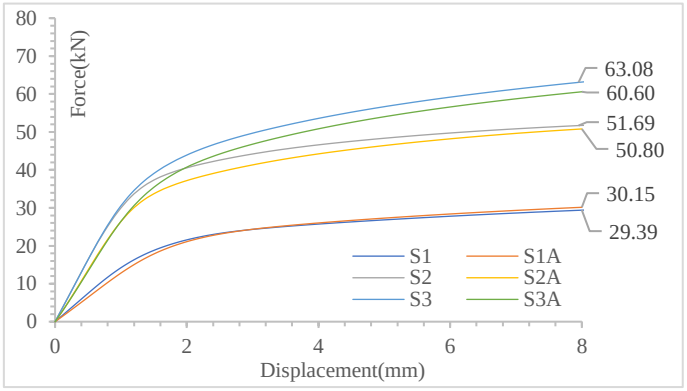

Fig. 24 Force-displacement curves of interlocking tie for h_2 = 2.0 m

5.2. Effect of wall thickness

As shown in Fig. 25, the hook shape in the 250 mm and 500 mm wall thickness schemes matches the empirical optimization scheme but is truncated at the bottom to accommodate the wall thickness while retaining the sawtooth area.

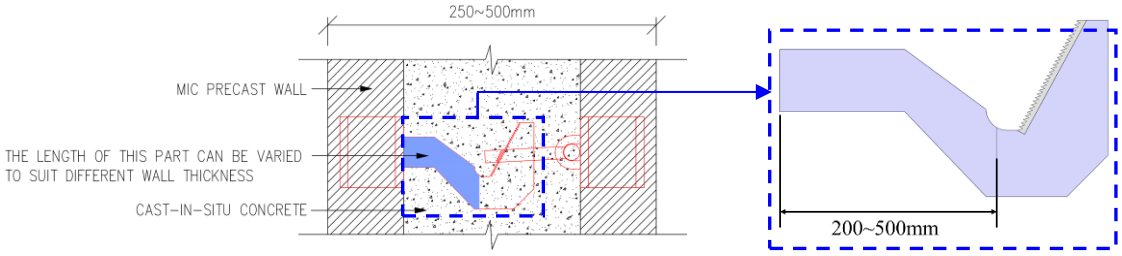

Fig. 25 Dimensions of interlocking tie for different wall-thicknesses (250 to 500 mm)

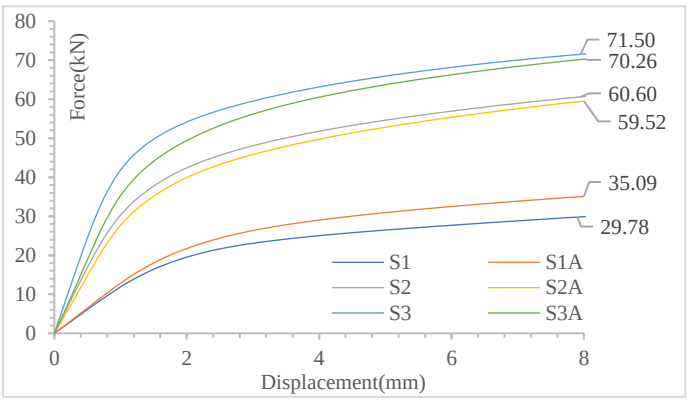

Fig. 26 Force-displacement curves of six load cases (wall thickness = 250mm)

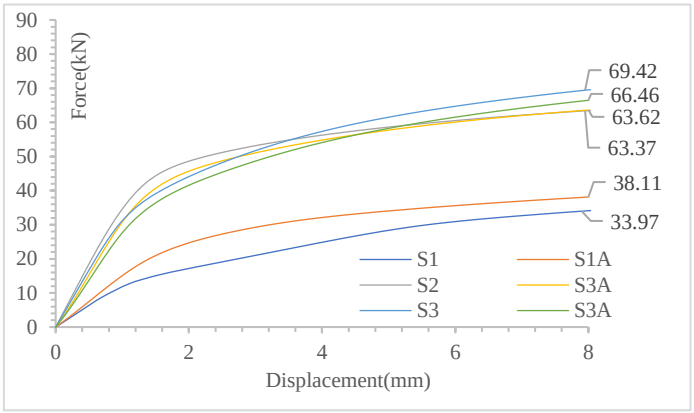

Fig. 27 Force-displacement curves of six load cases (wall thickness = 500mm)

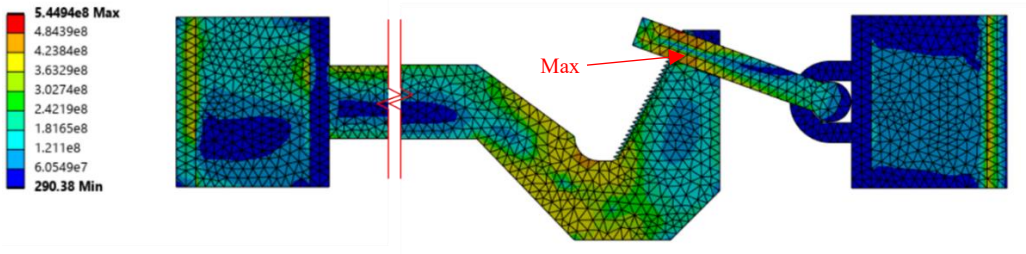

Fig. 28 Stress distribution at 8mm displacement for different wall thickness 250~500mm (S1)

As shown in Fig. 26, for a wall thickness of 250 mm, the tensile force of the wall tie at 8 mm displacement is 96.1% of that in the empirical scheme. The reduction in strength is primarily due to the increased moment on the support plates, caused by the change in the lever arm.

As shown in Fig. 27, for a wall thickness of 500 mm, the tensile force of the wall tie at 8 mm displacement is nearly identical to that in the empirical scheme. This is because the root of the hook is relatively strong compared to other parts of the system and remains elastic under the 8 mm displacement load. The typical stress distribution of the interlocking tie in different wall thickness for Case S1 is shown in Fig. 28.

6. Application in a Hong Kong MiC project

After the optimizations, the design of the interlocking tie system was finalized and incorporated into a four-story reinforced concrete MiC project in Hong Kong, as shown in Fig. 29. The optimized dimensions facilitated easier manufacturing and installation in the factory, minimizing conflicts with on-site rebar placement. The complete design received approval from local regulatory authorities. The project consisted of 106 MiC modules, including 90 composite walls, and featured a total of 1,048 inner tie sets. With the deformation of the sidewalls effectively controlled by the inner ties, the on-site concrete pouring for each composite wall proceeded successfully.

In comparison to the traditional method of using through-bolts to penetrate precast sidewalls, the use of inner ties resulted in a time savings of approximately one month and a reduction in construction costs by several million HKD for this project.

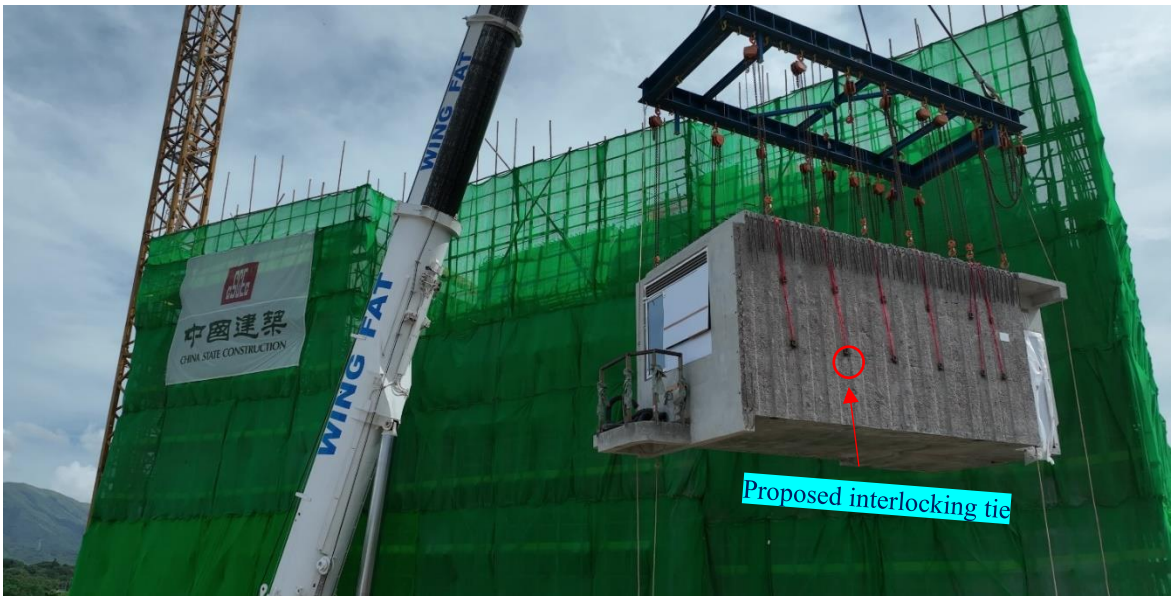

Fig. 29 Proposed interlocking ties adopted in a MiC building

7. Conclusions

This paper introduces an innovative interlocking tie system to address the challenge of securing prefabricated sidewalls during concrete casting in composite walls for reinforced concrete modular integrated construction (MiC) projects. The study utilizes topology optimization via software ANSYS to refine the interlocking tie design, providing detailed descriptions of the optimization processes. This approach minimizes material usage while improving manufacturing and installation efficiency. A comparison between topology optimization results and those from empirical optimization based on finite element analysis (FEA) reveals an average difference in mechanical properties of less than 5%. This demonstrates that empirical optimization is a viable and resource-efficient alternative in engineering practice.

To accommodate project-specific variations such as interlocking tie positioning and wall thickness, the study investigates interlocking ties with lower bearing capacities and varying wall thicknesses. The results show that interlocking ties can effectively control sidewall deformation across various scenarios through simple dimensional adjustments.

The optimized interlocking tie system was successfully implemented in a real MiC project in Hong Kong, providing a valuable reference for future initiatives. This innovative system could enhance the rate of interior decoration in high-rise buildings. The dimensions of the interlocking ties can be customized to accommodate various wall thicknesses and heights above floor level.

In the future, through further fire resistance and durability tests, this system may also be used for permanent tie connections between precast sidewalls and cast-in-situ walls, thus enhancing the overall stiffness of the structure and further reducing the total thickness of the structural walls.

Acknowledgments

The R&D funding support for “Research on Key Connections of Reinforced Concrete Modular Integrated Construction Structures” from China State Construction Engineering (Hong Kong) Limited is gratefully acknowledged. We would like to express our sincere gratitude to Dr Jianwei HE from NIDA Technology Co., Ltd. for providing valuable suggestions for this research. We would also like to extend our heartfelt thanks to Zhongcai HE, Chenghua HE, Daniel KAN, Yang ZHANG and Chimun LO for site supervision during MiC construction in a Hong Kong project. Lastly, we would like to thank Haoyue QIAO for proofreading.

References

[1] Bendsøe, M.P. (1989). Optimal shape design as a material distribution problem. Structural Optimization, 1:193–202.

[2] Bendsøe, M.P., Sigmund, O. (1999). Material interpolation schemes in topology optimization. Archive of Applied Mechanics, 69:635-654.

[3] Bendsoe, M.P., Sigmund, O. (2004). Topology optimization: theory, methods and applications. Springer, Berlin.

[4] Chen, L.Q. (2002). Phase-field models for microstructure evolution. Annual Review of Materials Research, 32:113-140.

[5] Clear, C. A., Harrison, T. A. (1985). CIRIA Report 108 - Concrete Pressure on Formwork. Construction Industry Research and Information Association, London.

[6] Deaton, J.D., Grandhi, R.V. (2014). A survey of structural and multidisciplinary continuum topology optimization: post 2000. Structural and Multidisciplinary Optimization, 49:1-38.

[7] Duan, L.J., Yu, Y.S., Wang, T., et al. (2022). Experimental research on mechanical behavior of Prefabricated Prefinished Volumetric Construction connections. Journal of Qingdao University of Technology, vol. 43, no. 5, pp. 1-7.

[8] Hu, H.S., Xia, H.J. (2023). A type of modular shear wall structure and its construction method. CN115807499B[P], 2023-04-25.

[9] Ji, J., Huang, G.X., Feng, Z.H., et al. (2022). A type of composite modular integrated construction structure. CN115045534A[P], 2022-09-13.

[10] Kobayashi, M.H. (2010). On a biologically inspired topology optimization method. Communications in Nonlinear Science and Numerical Simulation, 15(3):787-802.

[11] Li, Z., Wang, Q., Zhang, J.Y., et al. (2023). A type of MiC building with mixed wall structures. CN219794297U[P], 2023-10-03.

[12] Osher, S., Sethian, J.A. (1988). Fronts propagating with curvature dependent speed: algorithms based on the Hamilton-Jacobi formulation. Journal of Computational Physics, 79(1):12-49.

[13] Pan, W., Wang, Z., Zhang, Y., et al. (2023). Horizontal connection joint and construction method of multi-story and high-rise concrete MiC buildings. CN116084591A[P], 2023-05-09.

[14] Poon, C.M., Ma, M.C., Li, Z., et al. (2023). A type of concrete MiC structural system and its construction mete hod. CN117127714A[P], 2023-11-28.

[15] Rozvany, G.I.N., Zhou, M., Birker, T. (1992). Generalized shape optimization without homogenization. Structural Optimization, 4:250-252.

[16] Stolpe, M., Svanberg, K. (2001). An alternative interpolation scheme for minimum compliance topology optimization. Structural and Multidisciplinary Optimization, 22:116-124.

[17] Svanberg, K. (1987). The method of moving asymptotes—a new method for structural optimization. International Journal for Numerical Methods in Engineering, 24:359-373.

[18] Svanberg, K. (2002). A class of globally convergent optimization methods based on conservative convex separable approximations. SIAM Journal on Optimization, 12(2):555-573.

[19] Xie, Y.M., Steven, G.P. (1993). A simple evolutionary procedure for structural optimization. Computers & Structures, 49(5):885-896.

[20] Xie, Y.M., Steven, G.P. (1997). Evolutionary structural optimization. Springer.

[21] Yao, J., Huang, M.Y., Zeng, Z.X., et al. (2023). A type of concrete MiC module. CN219527957U[P], 2023-08-15.

[22] Zhou, M., Rozvany, G.I.N. (1991). The COC algorithm, Part II: topological, geometrical and generalized shape optimization. Computer Methods in Applied Mechanics and Engineering, 89:309-336. https://doi.org/10.1016/0045-7825(91)90046-9

[23] Zhou, M., Rozvany, G.I.N. (2001). On the validity of ESO type methods in topology optimization. Structural and Multidisciplinary Optimization, 21:80-83.

[24] Zillober, C. (1993). A globally convergent version of the method of moving asymptotes. Structural Optimization, 6:166-174.

[25] Zou, X.K., Huang, J., Lu, W.J., et al. (2024). A New Composite Wall Inner Tie System Applied in Reinforced Concrete Modular Integrated Construction. Proceedings of the 10th International Conference on Construction Engineering and Project Management, pp. 85-92, Jul. 29-Aug.1, Sapporo.

[26] Zou, X.K., Chan, C.M., Li, G., Wang, Q. (2007). Multi-objective Optimization for Performance-Based Design of Concrete Structures. Journal of Structural Engineering, vol. 133, vol. 10, pp. 1462-1474.

[27] Zou, X.K., Zhang, Y., Liu, Y.P., Shi, L.C., Kan, D. (2023). Design and Construction of High-Performance Long-Span Steel Transfer Twin Trusses Applied in One Hospital Building in Hong Kong. Buildings, vol. 13, no. 3:751.